Mooring observed mode-2 internal solitary waves in the northern South China Sea

Liang Chen[1, 2, 3*], Xuejun Xiong[1, 2, 3*], Quanan Zheng[4], Yeli Yuan[1, 2, 3], Long Yu[1, 2, 3], Yanliang Guo[1, 2, 3], Guangbing Yang[1, 2, 3], Xia Ju[1, 2, 3], Jia Sun[1, 2, 3], Zhenli Hui[1, 2, 3]

[1] First Institute of Oceanography, Ministry of Natural Resources, Qingdao 266061, China

[2] Founctional Laboratory for Regional Oceanography and Numerical Modeling, Pilot National Laboratory for Marine Science and Technology (Qingdao), Qingdao 266237, China

[3] Laboratory for Regional Oceanography and Numerical Modeling, Pilot National Laboratory for Marine Science and Technology (Qingdao), Qingdao 266237, China

[4] Department of Atmospheric and Oceanic Science, University of Maryland, College Park, Maryland 20742, USA

Abstract

The mode-2 internal solitary waves (ISWs) generated by mode-2 internal tide (IT) are identified by mooring observations in the northern South China Sea (SCS) from 2016 to 2017. Two mode-2 ISWs with a re-appearance period of 24.9 h observed on 29 and 30 July 2016 are characterized by type-b ISWs. They occurred when the isotherms compressed obviously in the vertical direction. Modal decomposition of IT horizontal currents shows that the vertical compression of the isotherms is mainly caused by diurnal mode-2 IT. The analysis of the role of the density stratification reveals that a deeper and thinner pycnocline is favorable for generation of mode-2 ISWs rather than pycnocline intensity. By comparing the mode-2 nonlinear, dispersion coefficients and the Ursell numbers calculated based on the stratification associated with different kinds of ITs with the observation results, it is shown that the diurnal mode-2 IT plays a crucial role in the generation of the mode-2 ISWs. When the diurnal mode-2 IT interacts with the semidiurnal IT and causes a deeper and thinner pycnocline, the mode-2 ISWs are easily excited.

Key words: mode-2 internal solitary waves, South China Sea, internal tide, mooring observation

1 Introduction

Previous investigations have shown that the internal solitary waves (ISWs), with large amplitudes and strong current velocities, are broadly distributed in the stratified coastal ocean and marginal seas (Jackson, 2007; Zhao et al., 2006; Stanton and Ostrovsk, 1998; Apel et al., 1985; Osborne and Burch, 1980). The South China Sea (SCS), in particular the northern SCS, is one of ocean areas where the energetic ISWs occur frequently (Wang et al., 2013; Zheng, 2017; Chen et al., 2018). In terms of the wave modes, the observed ISWs in the northern SCS could be categorized as two types, i.e., the first baroclinic mode (mode-1) and the second baroclinic mode (mode-2) (Yang et al., 2004; Chen et al., 2019). Mode-1 ISWs are characterized by only one extreme value of the vertical displacement of isotherms in the whole water column. Mode-2 ISWs typically show upward (downward) displacement of isotherms in the upper (lower) water column and three layers of currents from the uppermost to bottommost portions of a wave (Yang et al., 2010). In recent years, mode-2 ISWs

in the northern SCS have been observed and reported (Yang et al., 2004; 2009; Ramp et al., 2012). According to mooring observations, Yang et al. (2009) found that mode-2 ISWs on the upper continental slope of the northern SCS occur occasionally in summer, and more frequently in winter, implying that their occurrence may be associated with the seasonal change of local stratification. Ramp et al. (2015) observed a profusion of mode-2 ISWs during 5–16 August 2011 by two cruises. They found that the waves cannot persist very far from the underwater ridge and likely do not contribute to the SCS transbasin wave phenomenon. Most recently, Chen et al. (2019) revealed a high occurrence frequency of mode-2 ISWs (including 21 mode-2 ISWs) on the northwestern SCS shelf slope west of Dongsha Atoll in December 2016, and reported an extreme mode-2 ISW with maximum upward and downward amplitudes of 73 m and 91 m, respectively. This implies that the mode-2 ISWs present in the SCS and are not difficult to be observed. Although the amplitudes and current velocities of mode-2 ISWs are smaller than those of the mode-1

ISWs, the strong currents induced by mode-2 ISWs occur in deeper water layers. Therefore, they may cause a severer threat to the underwater operation of offshore engineering, underwater navigation, and acoustic communication. Moreover, the vertical shear of the horizontal current associated with mode-2 ISWs can reach as large as 0.045 s^{-1}, which is about 2 times that of the typical mode-1 ISWs (Qian et al., 2016). This may cause a stronger vertical mixing.

Nonlinearization of internal tide (IT) has been proved to be one of the main mechanisms for the generation of ISWs in the northern SCS. Zhao (2014) found the coherence of horizontal distribution of ISW packets observed from the SAR images with the energy fluxes of the northwestward mode-1 M$_2$ ITs, which provides solid evidence for the scenarios that the ISWs in the northeastern SCS deep basin originate from M$_2$ ITs at the western Luzon Strait, while the diurnal ITs play a secondary role by modifying the ISW generation (Buijsman et al., 2010; Helfrich and Grimshaw, 2008; Li and Farmer, 2011; Zhang et al., 2011). Most previous studies of the ITs in the northern SCS were restricted from the Luzon Strait to the Dongsha Atoll in the northeastern SCS but few on the continental shelf far away from the west of Dongsha Atoll, and focused on the mode-1 motions in this area (Duda et al., 2004; Yang et al., 2004; Xu et al., 2014). Based on 8-month moored acoustic Doppler current profiler observations on the northwestern SCS shelf slope west of the Dongsha Atoll, Xu et al. (2013) demonstrates that the diurnal IT are dominated by the first mode, whereas the semidiurnal tides show a variable multimodal structure: the mode-2 is dominant in summer and comparable to the first mode in spring and autumn, but the mode-1 predominates in winter.

For the generation mechanisms of mode-2 ISWs, previous studies have shown that they could be generated by the interaction between the mode-1 ISWs and topography (Helfrich and Melville, 1986; Vlasenko and Hutter, 2001; Guo and Chen, 2012; Liu et al., 2013; Lamb and Warn-Varnas, 2015) or the changes in the stratification induced by internal tides (ITs) and mesoscale eddies (Grisouard et al., 2011; Chen et al., 2014; Dong et al., 2016; Liang and Li, 2019). By laboratory experiments, Vlasenko and Hutter (2001) found that mode-1 ISWs can break into two types of ISWs, i.e., mode-1 and mode-2 ISWs, when they encounter an underwater sill. The simulative results by a two-dimensional numerical model show that both convex and concave mode-2 ISWs could be evolved from the shoaling mode-1 ISWs on the continental shelf (Lamb and Warn-Varnas, 2015). Synthetic aperture radar images show that eddy-induced change of the water stratification can result in favorable hydrographic conditions for internal wave generation (Dong et al., 2016). The resonance between mode-1 ITs and anticyclonic eddy excites mode-2 ITs, then the mode-2 ITs disintegrate into mode-2 ISWs (Dong et al., 2016). However, there have been few field observations for mode-2 ISWs generation. In this study, the mechanism of mode-2 ISWs generated by mode-2 ITs is identified by one year of mooring observations in the northern SCS from 2016 to 2017.

2 Data and methods

2.1 *Mooring observation and data*

During the period from 30 June 2016 to 21 July 2017, a subsurface mooring, specially designed for observing ocean internal waves, was deployed to monitor the current velocity, the temperature and the salinity on the continental shelf slope west of Dongsha Atoll in the northern SCS. The mooring system was located at depth of 397 m as shown in Fig. 1. The current velocity was sampled via a 40-inch vitreous mounted, upward-looking 75 kHz acoustic-doppler-current-profile (ADCP) at depth of 380 m,
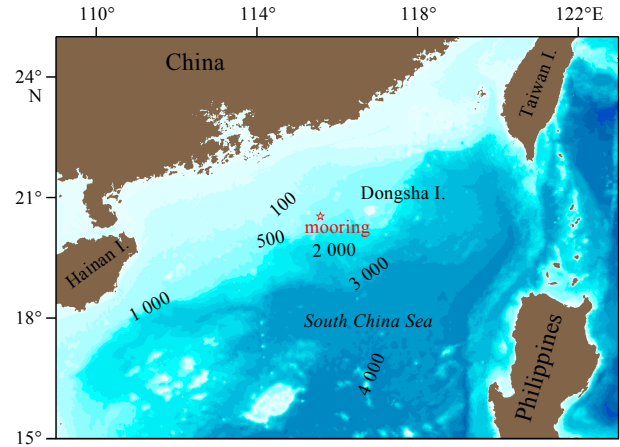

Fig. 1. Topography of the study area and mooring location (red star). Numerals on isobaths are in m.

17 m above the bottom. It sampled 8-m bins every 3 min from 29 June 2016 to 13 June 2017 with a three-month gap from 20 November 2016 to 20 February 2017 due to battery failure. The depth of available current data measured by ADCP ranged from 43 m to 363 m. The vertical oscillations of the ADCP are very small, which can be ignored, because the installation depth of ADCP is close to the seabed. Between depths of 50 m and 380 m, a thermistor chain consisting of temperature loggers at every 10 m and conductivity-temperature-depth (CTD) instruments at every 50 m were attached to the mooring to monitor the temperature and the salinity every 3 min. The depths of the temperature loggers are obtained by interpolation of the depths measured by CTDs.

2.2 *Internal tidal currents*

The horizontal current induced by the ITs can be calculated by

$$u_{IT}(z, t) = u_t(z, t) - u_{ht}(t), \qquad (1)$$

where $u_t(z, t)$ is the horizontal tide current, which can be obtained by harmonic analysis of ADCP observed currents. $u_{ht}(t)$ is the barotropic tide current, which can be calculated by $u_{ht}(t) = \dfrac{1}{H} \int_{-H}^{0} u_t(z, t) \mathrm{d}z$, where H is the depth. The internal tidal currents were band-pass filtered to separate diurnal (0.85 K$_1$–1.15 O$_1$) and semidiurnal (0.85 M$_2$–1.15 S$_2$) motions via a fourth-order Butterworth filter (Xu et al., 2013; 2014).

2.3 *Modal decomposition of the ITs*

In a continuous stratified fluid, the vertical structure of the vertical displacement Φ_n can be described as the eigenmode equation:

$$\frac{\mathrm{d}^2 \Phi_n}{\mathrm{d}z^2} + \frac{N^2(z)}{c_n^2} \Phi_n = 0, \qquad (2)$$

$$\Phi(-H) = \Phi(0) = 0, \qquad (3)$$

where $N^2(z) = -\dfrac{g}{\rho} \dfrac{\mathrm{d}\rho}{\mathrm{d}z}$ is the buoyancy frequency, c_n is the linear wave speed. The vertical structure of horizontal velocity Π_n can be written as

$$\Pi_n\left(z\right) \propto \frac{\mathrm{d}\Phi_n}{\mathrm{d}z}. \tag{4}$$

The horizontal current induced by the IT can be approximately expressed as

$$u_{\mathrm{IT}}\left(z,t\right) = \sum_{n=1}^{4} u_n\left(t\right) \Pi_n\left(z\right), \tag{5}$$

where $u_n\left(t\right)$ is the time-varying magnitude of the IT horizontal velocity of mode n. $u_{\mathrm{IT}}\left(z,t\right)$ can be extracted by Eq. (1). $\Pi_n\left(z\right)$ can be calculated by Eqs (2)–(4). According to Eq. (5), we make a modal decomposition of the amplitude of the IT horizontal velocity using the least square method. Thus, $u_n\left(t\right)$ can be written as

$$u_n\left(t\right) = \left(\Pi_n^{\mathrm{T}}\Pi_n\right)^{-1}\Pi_n^{\mathrm{T}}u_{\mathrm{IT}}, \tag{6}$$

where Π_n^{T} is the transpose of Π_n.

Finally, the horizontal IT velocity of mode n can be written as

$$u_n\left(z,t\right) = u_n\left(t\right) \Pi_n\left(z\right). \tag{7}$$

The depth-integrated horizontal kinetic energy (HKE) of mode n IT can be expressed as

$$\mathrm{HKE}_n = \frac{1}{2}\int_{-H}^{0} \rho\left(z\right) u_n^2\left(z,t\right) \mathrm{d}z. \tag{8}$$

3 Results and discussion

3.1 *Mode-2 ISWs*

Figure 2 shows two mode-2 ISWs observed on 29 and 30 July 2016, which are named No. 1 mode-2 ISW and No. 2 mode-2 ISW, respectively. No. 1 mode-2 ISW started at 17:48 and ended at 18:24 on 29 July 2016, and No. 2 mode-2 ISW started at 18:30 and ended at 19:21 on 30 July 2016. The peaks of the two mode-2 ISWs occurred at 18:06 and 19:00, respectively, indicating that the re-appearance period of them is 24.9 h, which is a characteristic time scale of type-b ISWs (Ramp et al., 2004; Chen et al., 2019). It is worth noting that the isotherms in the layer above the depth of 140 m start to sink, while the isotherms in the layer below start to rise at 13:00 on 29 July 2016. No. 1 mode-2 ISW occurred when the isotherms in the upper layer sunk deeper and the isotherms in the lower layer rose higher. No. 2 mode-2 ISW also occurred under similar hydrographic conditions. Because the re-appearance period of the two mode-2 ISWs is 24.9 h, which is close to the period of lunar day, implying that the occurrences of the two mode-2 ISWs may be associated with the IT which cause the isotherms to be compressed vertically.

3.2 *Characteristics of ITs*

In order to determine the IT features when the mode-2 ISWs occur, we extract the horizontal current induced by the IT using the ADCP data. As shown in Fig. 3b, the color contours represent the zonal currents induced by the IT calculated by Eq. (1). The dashed lines are the band-pass filter isotherms induced by diurnal and semidiurnal ITs. The cut frequency of the diurnal and semidiurnal ITs were set to [0.85 K_1–1.15 O_1] and [0.85 M_2–1.15 S_2], respectively. In order to determine the occurrence time of the mode-2 ISWs, the isotherms of 26°C and 18°C are shown in Fig. 3a. The red dotted lines are the starting time of the mode-2 ISWs. One can see that the mode-2 ISWs occur when the band-pass filter isotherms are significantly compressed, i.e., the upper isotherms are concave and the lower isotherms are convex. The zonal velocities induced by the IT show a three-layer structure with two turning points at depths of 80 m and 230 m at the time of mode-2 ISWs occurrence. These results reveal that the mode-2 ISWs occur when the isotherms significantly compressed caused by the mode-2 IT.

In order to find out whether the observed mode-2 IT signals come from the semidiurnal IT or diurnal IT, we make modal de-
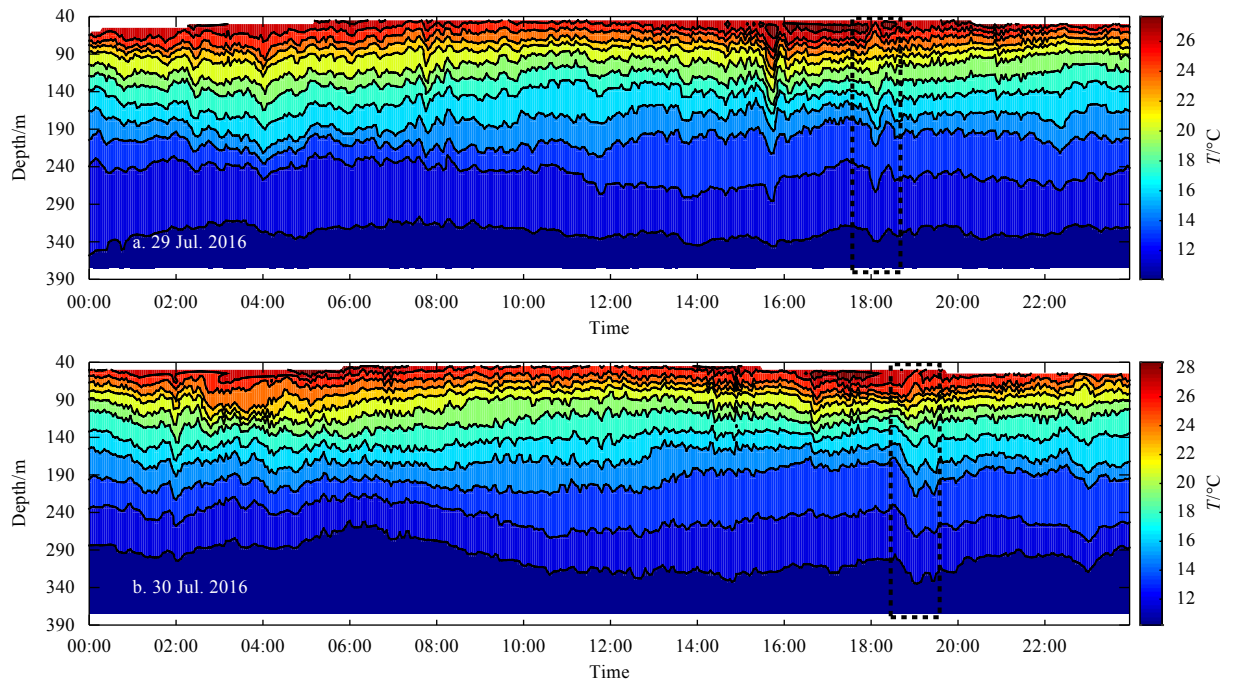

Fig. 2. Temperature profiles observed by the mooring on 29 (a) and 30 (b) July 2016. Mode-2 ISWs are marked by dotted boxes.
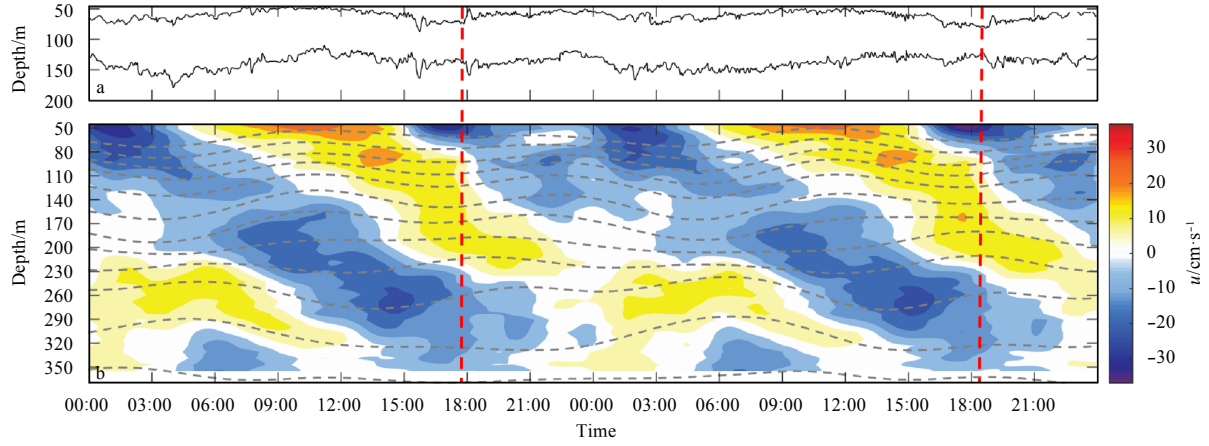
Fig. 3. Time series of IT current profile from 29 to 30 July 2016. a. Upper and lower curves are time series isotherms of 26°C and 18°C, respectively. b. Color contours represent the zonal currents induced by the IT. The dashed lines are the band-pass filter isotherms. Red dashed lines represent the starting times of the mode-2 ISWs.

composition of the total, semidiurnal and diurnal ITs, respectively. Figures 4b–d show the depth-integrated horizontal kinetic energy (HKE) of different modes of total, diurnal and semidiurnal IT currents, respectively. As shown in Fig. 4b, at the onset time of No. 1 and No. 2 mode-2 ISWs, the depth-integrated HKE of mode-2 IT currents is the largest component in the total HKE. This indicates that mode-2 ISWs occur concurrently with mode-2 ITs. The depth-integrated HKE of diurnal and semidiurnal IT currents as shown in Figs 4c and d show that the mode-2 ISWs occurred at the time when the depth-integrated HKE of diurnal mode-2 IT currents reached their maximum values, instead of semidiurnal IT. Figures 5b–e show time series of zonal velocity profiles induced by diurnal IT modes 1–4 derived from mooring data. One can also see that the mode-2 ISWs do occur when the diurnal mode-2 IT is dominate. These results indicate that mode-2 ISWs occur concurrently with the diurnal mode-2 IT.

3.3 *Influences of density stratification on generation of mode-2 ISWs*

Previous investigation has shown that mode-2 ISWs can be well described by KdV equation (Chen et al., 2019). In a continuous stratified fluids, the KdV equation can be written as (Pelinovsky et al., 2007)

$$\frac{\partial \eta_n}{\partial t} + c_n \frac{\partial \eta_n}{\partial x} + \alpha_n \eta_n \frac{\partial \eta_n}{\partial x} + \beta_n \frac{\partial^3 \eta_n}{\partial x^3} = 0, \tag{9}$$

where c_n, α_n, β_n are the linear wave speed, nonlinear coefficient and dispersion coefficient of mode n, respectively. Here

$$\alpha_n = \frac{3c_n}{2} \int_{-H}^{0} \frac{\mathrm{d}^3 \Phi_n}{\mathrm{d}z^3} \mathrm{d}z \bigg/ \int_{-H}^{0} \frac{\mathrm{d}^2 \Phi_n}{\mathrm{d}z^2} \mathrm{d}z, \tag{10}$$
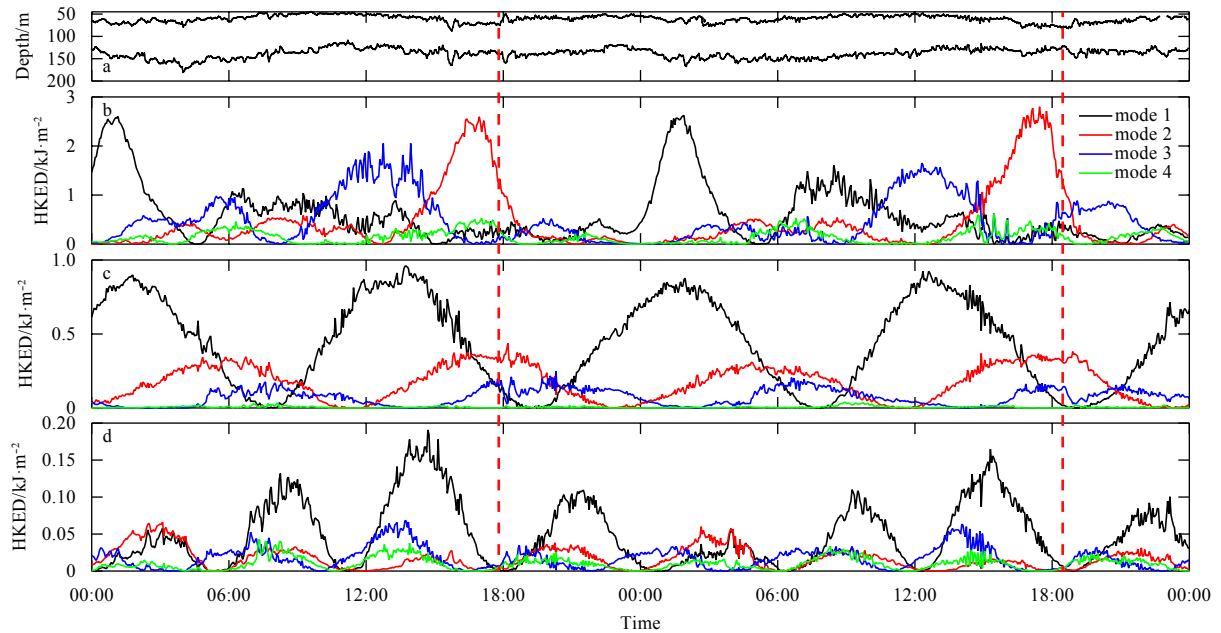

Fig. 4. Time series (from 29 to 30 July 2016) of 26°C and 18°C isotherms (a), and depth-integrated HKE of different modes of total (b), diurnal (c) and semidiurnal (d) IT currents, respectively. Red dashed lines represent the starting times of the mode-2 ISWs.
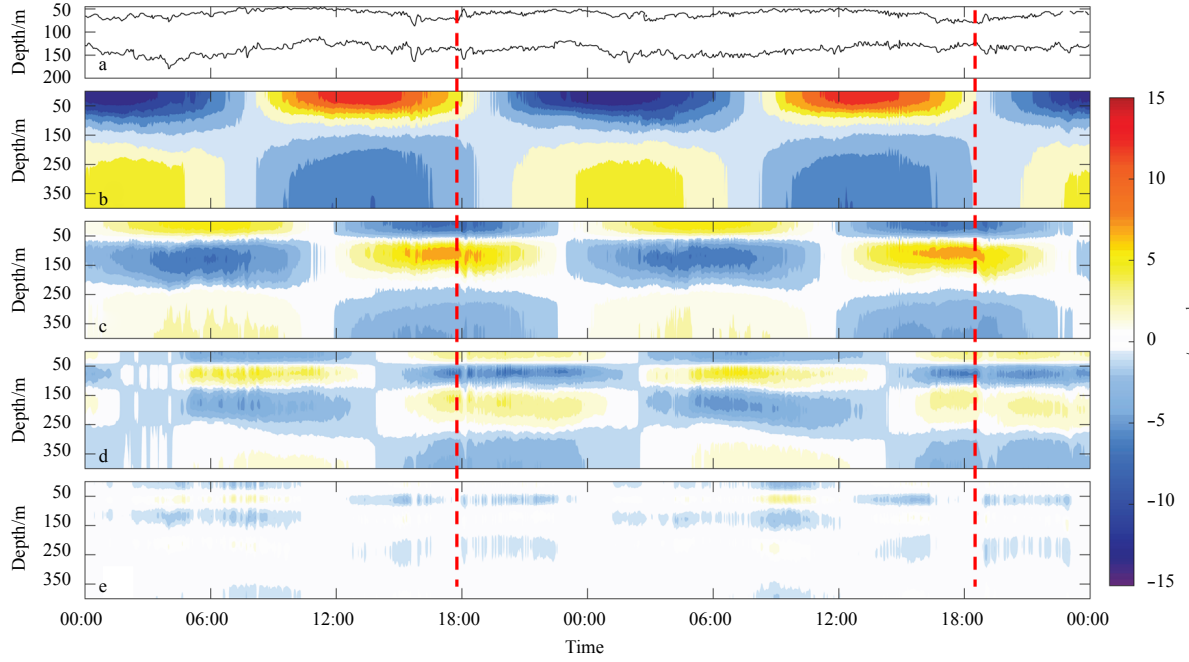
Fig. 5. Time series (from 29 to 30 July 2016) of 26°C and 18°C isotherms (a), and zonal velocity profiles induced by diurnal IT of modes 1–4 (b–e), respectively. Red dashed lines represent the starting times of the mode-2 ISWs.

$$\beta_n = \frac{c_n}{2} \int_{-H}^{0} \Phi_n^2 \mathrm{d}z \Big/ \int_{-H}^{0} \frac{\mathrm{d}^2 \Phi_n}{\mathrm{d}z^2} \mathrm{d}z, \tag{11}$$

where Φ_n can be calculated by Eqs (2) and (3).

Nonlinear coefficient α_n and dispersion coefficient β_n are environmental parameters determined by ocean stratification and water depth, which are related to the generation of ISWs. For example, a deeper and thinner pycnocline may change the sign of nonlinear coefficient α_1, and the elevation ISWs were expected to be evolved from the ITs (Xu et al., 2010).

The Ursell number is defined as

$$U_n = \alpha_n/\beta_n. \tag{12}$$

The larger the U_n, the easier the ISWs will be generated (Yang et al., 2009).

The density stratification profile can be approximately described by hyperbolic tangent function according to mooring data (Wang, 2006).

$$\rho(z) = \rho_0 \exp\left\{\frac{\Delta\rho}{2\rho_0} \tanh\left[\frac{-2(z+d)}{\delta}\right]\right\}, \tag{13}$$

where ρ_0 is the sea surface water density, $\Delta\rho$ is the density difference between the upper and lower bounds of the pycnocline, d is the pycnocline depth, δ is the pycnocline thickness. The corresponding buoyancy frequency is given by

$$N^2(z) = -\frac{g}{\rho}\frac{\mathrm{d}\rho}{\mathrm{d}z} = \frac{g\Delta\rho}{\delta\rho_0}\operatorname{sech}^2\left[\frac{2(z+d)}{\delta}\right]. \tag{14}$$

The three parameters $\Delta\rho$, d and δ determine the density stratifiation profile as shown in Fig. 6. According to the above analysis results, the two mode-2 ISWs occurred when the isotherms signi-
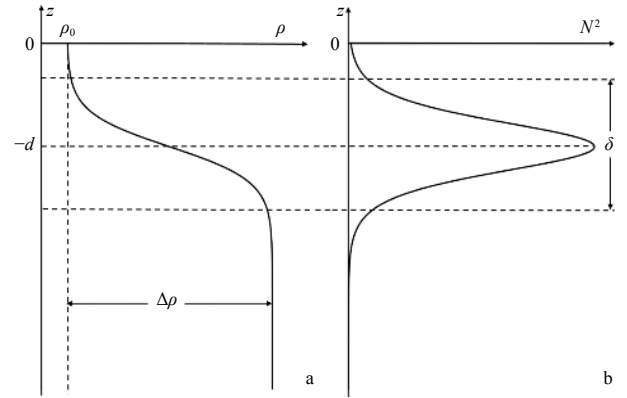

Fig. 6. Ideal vertical profiles of the density (a) and buoyancy frequency (b) with parameter definitions.

ficantly compressed caused by mode-2 IT. In fact, the concave upper isotherm and convex lower isotherm imply that the depth of the thermocline sinks, the thickness of the thermocline becomes thinner and the strength of the thermocline increases. Therefore, we use the control variable method to calculate the distribution of mode-2 environmental parameters α_2, β_2 and U_2 with the pycnocline depth d, the pycnocline thickness δ and the pycnocline intensity $\Delta\rho/\delta$. The calculation results are shown in Fig. 7. One can see that (1) as the pycnocline depth becomes deeper, the nonlinear coefficient α_2 increases, the dispersion coefficient β_2 increases first and then decreases, and the Ursell number U_2 increases, implying that mode-2 ISWs are more easily generated with the deepening of the pycnocline depth; (2) as the pycnocline becomes thicker, the nonlinear coefficient α_2 increases, the dispersion coefficient β_2 decreases, and the Ursell number U_2 decreases rapidly, implyingthat the thicker the pycnocline, the more difficult to generate mode-2 ISWs; (3) as the
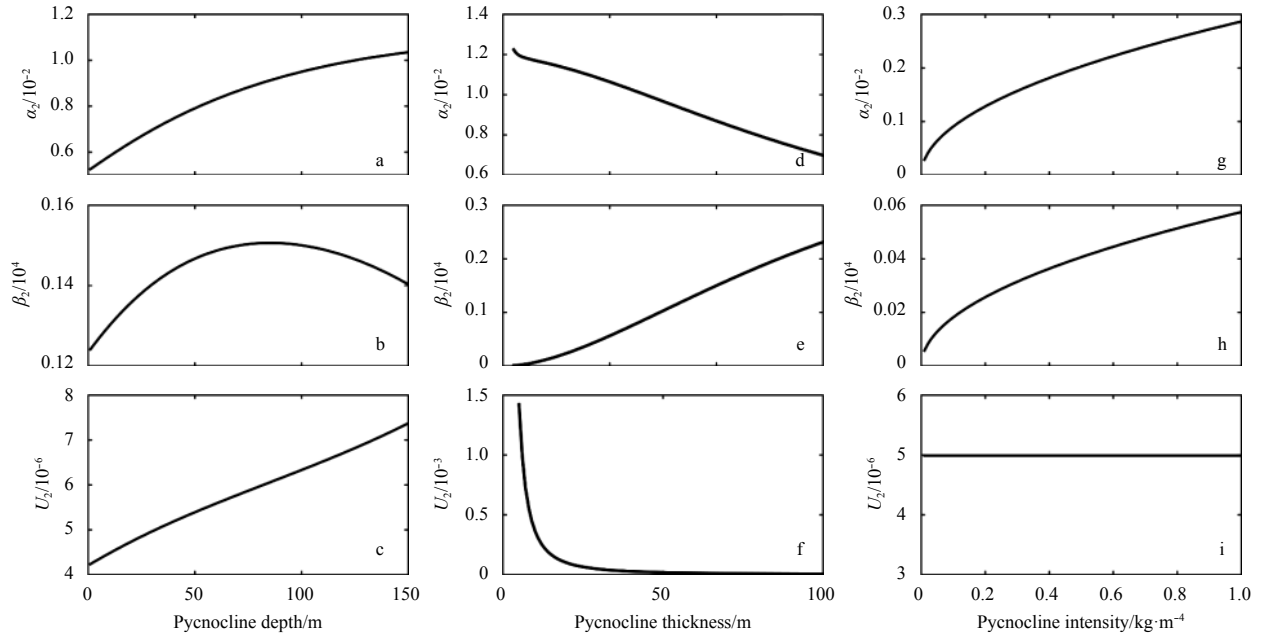
Fig. 7. Variability of mode-2 environmental parameters α_2 (a, d, g), β_2 (b, e, h) and U_2 (c, f, i) with the pycnocline depth d (a–c), the pycnocline thickness δ (d–f) and the pycnocline intensity $\Delta\rho/\delta$ (g–i).

pycnocline intensity increases, nonlinear coefficient α_2 and dispersion coefficient β_2 increase, and the Ursell number almost unchanged, implying that the variation of pycnocline intensity has no effect on the generation of mode-2 ISWs.

The results show that a deeper and thinner pycnocline is a favorable condition for the generation of mode-2 ISWs. But the pycnocline intensity has little effect on the emergence of mode-2 ISWs. This is consistent with the numerical simulation results by Chen et al. (2014). During the observation period from 29 June 2016 to 21 July 2017, there were 42 mode-2 ISWs observed at the mooring station. More than 64% of them occurred in winter and only 14% of them occurred in summer. Because the pycnocline in the SCS is deeper in winter than that in summer, the occurrence frequency of mode-2 ISWs in the SCS in winter is much higher than that in summer. These results also explain why mode-2 ISWs are easily generated when the isotherms in the upper layer sunk deeper and the isotherms in the lower layer rose higher. Because, at the time, the pycnocline become deeper and thinner, favorable for the generation of mode-2 ISWs.

To further prove that the occurrence of the two mode-2 ISWs is related to the change of stratification and investigate the influence of the ITs on it, we calculate the mode-2 nonlinear, dispersion coefficients and the Ursell numbers with the varying stratification observed and associated with different kinds of ITs. The lack of stratification data near the surface is made up by the monthly data of World Ocean Atlas (WOA). As shown in Fig. 8, the black lines indicate the parameters calculated based on the observational stratification. Ignoring the anomalous value caused by the mode-1ISW occurred at around 16:30 on 30 July 2016, during the periods from 12:00 to 18:00 on 29 July and 13:00 to 18:30 on 30 July when mode-2 IT was the dominant component, the mode-2 Ursell number increases gradually till the mode-2 ISWs are generated. Combined with observational stratification and the results as shown in Fig. 7, it is shown that the observed mode-2 ISWs do occur at the stratified condition with a deeper and thinner pycnocline. The blue dashed lines indicate the parameters calculated based on the stratification associated

with semidiurnal internal tide. One can see that the variation of the three parameters calculated based on semidiurnal internal tidal stratification is basically consistent with the observational results. However, there is a significant phase difference between the extreme values of the parameters calculated based on semidiurnal internal tidal stratification and that of observation. The phase differences are particularly evident in the Ursell numbers at the onset time of the two mode-2 ISWs. The blue solid lines as shown in Fig. 8 indicate the parameters calculated based on the stratification associated with the semidiurnal IT and diurnal mode-2 IT. After considering the influence of the diurnal mode-2 IT on the stratification, the phase differences of the Ursell number at the onset time of the two mode-2 ISWs do not exist. In other words, the mode-2 ISWs occurred when the Ursell numbers reach their maximum values under the influence of the diurnal mode-2 IT. What's more, the maximum values of the Ursell number become bigger and more close to the observational results because of the influence of the diurnal mode-2 IT. These results indicate that when the diurnal mode-2 IT interacts with the semidiurnal IT and causes a deeper and thinner pycnocline, the mode-2 ISWs are easily excited. These results also explain why the re-appearance period of the two mode-2 ISWs is 24.9 h.

4 Summary

The generation mechanism of mode-2 ISWs is analyzed by mooring observations in the northern South China Sea (SCS) on 29 and 30 July 2016. Two mode-2 ISWs with a re-appearance period of 24.9 h, which is a typical feature of type-b ISWs, were observed. They occurred when the isotherms in the upper layer sunk deeper and the isotherms in the lower layer rose higher. Modal decomposition of IT horizontal currents shows that the vertical compression of the isotherms is mainly caused by diurnal mode-2 IT. The mode-2 ISWs occurred at the time when the depth-integrated HKE of diurnal mode-2 IT currents reached their maximum values, instead of semidiurnal IT. The analysis of the density stratification show that as the pycnocline becomes deeper and thinner, the mode-2 Ursell number increases, imply-
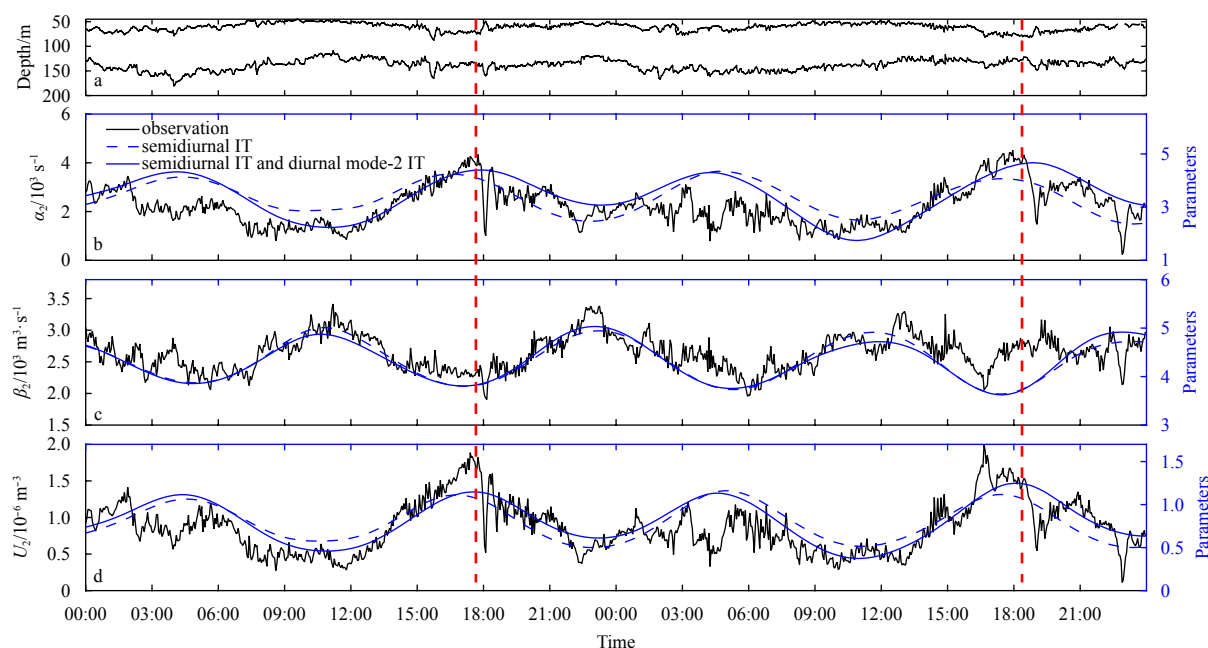
Fig. 8. Time series of 26°C and 18°C isotherms (a), and time series of mode-2 nonlinear coefficient (b), dispersion coefficient (c) and Ursell number (d) from 29 to 30 July 2016. The blue solid lines as shown in b–d indicate the parameters calculated based on the stratification associated with the semidiurnal IT and diurnal mode-2 IT. Red dashed lines represent the starting times of the mode-2 ISWs.

ing that a deeper and thinner pycnocline is favorable for the generation of mode-2 ISWs. However, as the pycnocline intensity increases, the mode-2 Ursell number is almost unchanged, implying that the generation of mode-2 ISWs is not directly related to the pycnocline intensity. By comparing the mode-2 nonlinear, dispersion coefficients and the Ursell numbers calculated by the stratification associated with different kinds of ITs with the observation results, it is shown that the variation of the three parameters calculated based on semidiurnal internal tidal stratification is basically consistent with the observational results. However, there is a significant phase difference between the extreme values of the parameters calculated based on semidiurnal internal tidal stratification and that of observation. The phase differences are particularly evident in the Ursell numbers at the onset time of the two mode-2 ISWs. Considering the influence of the diurnal mode-2 IT on the stratification, the phase differences of the Ursell number at the onset time of the two mode-2 ISWs do not exist. In other words, the mode-2 ISWs occurred when the Ursell numbers reach their maximum values under the influence of the diurnal mode-2 IT. What's more, the maximum values of the Ursell number become bigger and more close to the observational results because of diurnal mode-2 IT. These results indicate that when the diurnal mode-2 IT interacts with the semidiurnal IT and causes a deeper and thinner pycnocline, the mode-2 ISWs are easily excited. These results also explain why the re-appearance period of the two mode-2 ISWs is 24.9 h.

References

Apel J R, Holbrook J R, Liu A K, et al. 1985. The Sulu Sea internal soliton experiment. Journal of Physical Oceanography, 15(12): 1625–1651, doi: 10.1175/1520-0485(1985)015<1625:TSSISE>2.0.CO;2

Buijsman M C, Kanarska Y, McWilliams J C. 2010. On the generation and evolution of nonlinear internal waves in the South China Sea. Journal of Geophysical Research, 115(C2): C02012, doi:

10.1029/2009JC005275

Chen Zhiwu, Xie Jieshuo, Wang Dongxiao, et al. 2014. Density stratification influences on generation of different modes internal solitary waves. Journal of Geophysical Research: Oceans, 119(10): 7029–7046, doi: 10.1002/2014JC010069

Chen Liang, Zheng Quanan, Xiong Xuejun, et al. 2018. A new type of internal solitary waves with a re-appearance period of 23 h observed in the South China Sea. Acta Oceanologica Sinica, 37(9): 116–118, doi: 10.1007/s13131-018-1252-y

Chen Liang, Zheng Quanan, Xiong Xuejun, et al. 2019. Dynamic and statistical features of internal solitary waves on the continental slope in the northern South China Sea derived from mooring observations. Journal of Geophysical Research: Oceans, 124(6): 4078–4097, doi: 10.1029/2018JC014843

Dong Di, Yang Xiaofeng, Li Xiaofeng, et al. 2016. SAR observation of eddy-Induced mode-2 internal solitary waves in the South China Sea. IEEE Transactions on Geoscience and Remote Sensing, 54(11): 6674–6686, doi: 10.1109/TGRS.2016.2587752

Duda T F, Lynch J F, Irish J D, et al. 2004. Internal tide and nonlinear internal wave behavior at the continental slope in the northern South China Sea. IEEE Journal of Oceanic Engineering, 29(4): 1105–1130, doi: 10.1109/JOE.2004.836998

Grisouard N, Staquet C, Gerkema T. 2011. Generation of internal solitary waves in a pycnocline by an internal wave beam: A numerical study. Journal of Fluid Mechanics, 676: 491–513, doi: 10.1017/jfm.2011.61

Guo C, Chen X. 2012. Numerical investigation of large amplitude second mode internal solitary waves over a slope-shelf topography. Ocean Modelling, 42: 80–91, doi: 10.1016/j.ocemod.2011.11.003

Helfrich K R, Grimshaw R H J. 2008. Nonlinear disintegration of the internal tide. Journal of Physical Oceanography, 38(3): 686–701, doi: 10.1175/2007JPO3826.1

Helfrich K R, Melville W K. 1986. On long nonlinear internal waves over slope-shelf topography. Journal of Fluid Mechanics, 167: 285–308, doi: 10.1017/S0022112086002823

Jackson C. 2007. Internal wave detection using the Moderate Resolution Imaging Spectroradiometer (MODIS). Journal of Geophysical Research, 112(C11): C11012, doi: 10.1029/2007JC004220

Lamb K G, Warn-Varnas A. 2015. Two-dimensional numerical simulations of shoaling internal solitary waves at the ASIAEX site in the South China Sea. Nonlinear Processes Geophysics, 22: 289–312, doi: 10.5194/npg-22-289-2015

Li Q, Farmer D M. 2011. The generation and evolution of nonlinear internal waves in the deep basin of the South China Sea. Journal of Physical Oceanography, 41(7): 1345–1363, doi: 10.1175/2011JPO4587.1

Liang Jianjun, Li Xiaoming. 2019. Generation of second-mode internal solitary waves during winter in the northern South China Sea. Ocean Dynamics, 69(3): 313–321, doi: 10.1007/s10236-019-01246-6

Liu A K, Su Fengchun, Hsu Mingkuang, et al. 2013. Generation and evolution of mode-two internal waves in the South China Sea. Continental Shelf Research, 59: 18–27, doi: 10.1016/j.csr.2013.02.009

Osborne A R, Burch T L. 1980. Internal solitons in the Andaman Sea. Science, 208(4443): 451–460, doi: 10.1126/science.208.4443.451

Pelinovsky E, Polukhina O, Slunyaev A, et al. 2007. Internal solitary waves. In: Grimshaw R H J, ed. Solitary Waves in Fluids. Southampton, Boston: WIT Press, 85–110

Qian Hongbao, Huang Xiaodong, Tian Jiwei. 2016. Observational study of one prototypical mode-2 internal solitary waves in the northern South China Sea. Haiyang Xuebao (in Chinese), 38(9): 13–20

Ramp S R, Tang T Y, Duda T F, et al. 2004. Internal solitons in the northeastern South China Sea. Part I: Sources and deep water propagation. IEEE Journal of Oceanic Engineering, 29(4): 1157–1181, doi: 10.1109/JOE.2004.840839

Ramp S R, Yang Y J, Reeder D B, et al. 2012. Observations of a mode-2 nonlinear internal wave on the northern Heng-Chun Ridge south of Taiwan. Journal of Geophysical Research, 117(C3): C03043, doi: 10.1029/2011JC007662

Ramp S R, Yang Y J, Reeder D B, et al. 2015. The evolution of mode-2 nonlinear internal waves over the northern Heng-Chun Ridge south of Taiwan. Nonlinear Processes Geophysics, 22: 413–431, doi: 10.5194/npg-22-413-2015

Stanton T P, Ostrovsky L A. 1998. Observations of highly nonlinear internal solitons over the continental shelf. Geophysical Research Letters, 25(14): 2695–2698, doi: 10.1029/98GL01772

Vlasenko V I, Hutter K. 2001. Generation of second mode solitary waves by the interaction of a first mode soliton with a sill. Nonlinear Processes in Geophysics, 8(4): 223–239

Wang Gang. 2006. Numerical modelling on the generation process of the tidal internal waves over the northwestern South China Sea shelf (in Chinese) [dissertation]. Qingdao: Institute of Oceanology, Chinese Academy of Sciences

Wang Juan, Huang Weigen, Yang Jingsong, et al. 2013. Study of the propagation direction of the internal waves in the South China Sea using satellite images. Acta Oceanologica Sinica, 32(5): 42–50, doi: 10.1007/s13131-013-0312-6

Xu Zhenhua, Yin Baoshu, Hou Yijun, et al. 2010. A study of internal solitary waves observed on the continental shelf in the northwestern South China Sea. Acta Oceanologica Sinica, 29(3): 18–25, doi: 10.1007/s13131-010-0033-z

Xu Zhenhua, Yin Baoshu, Hou Yijun, et al. 2013. Variability of internal tides and near-inertial waves on the continental slope of the northwestern South China Sea. Journal of Geophysical Research: Oceans, 118(1): 197–211, doi: 10.1029/2012JC008212

Xu Zhenhua, Yin Baoshu, Hou Yijun, et al. 2014. Seasonal variability and north–south asymmetry of internal tides in the deep basin west of the Luzon Strait. Journal of Marine Systems, 134: 101–112, doi: 10.1016/j.jmarsys.2014.03.002

Yang Y J, Fang Y C, Chang M H, et al. 2009. Observations of second baroclinic mode internal solitary waves on the continental slope of the northern South China Sea. Journal of Geophysical Research: Oceans, 114(C10): C10003, doi: 10.1029/2009JC005318

Yang Y J, Fang Y C, Tang T Y, et al. 2010. Convex and concave types of second baroclinic mode internal solitary waves. Nonlinear Processes Geophysics, 17: 605–614, doi: 10.5194/npg-17-605-2010

Yang Y J, Tang T Y, Chang M H, et al. 2004. Solitons northeast of Tung-Sha Island during the ASIAEX pilot studies. IEEE Journal of Oceanic Engineering, 29(4): 1182–1199, doi: 10.1109/JOE.2004.841424

Zhang Z, Fringer O B, Ramp S R. 2011. Three-dimensional, nonhydrostatic numerical simulation of nonlinear internal wave generation and propagation in the South China Sea. Journal of Geophysical Research: Oceans, 116(C5): C05022, doi: 10.1029/2010JC006424

Zhao Zhongxiang. 2014. Internal tide radiation from the Luzon Strait. Journal of Geophysical Research: Oceans, 119(8): 5434–5448, doi: 10.1002/2014JC010014

Zhao Zhongxiang, Alford M H. 2006. Source and propagation of internal solitary waves in the northeastern South China Sea. Journal of Geophysical Research, 111(C11): C11012, doi: 10.1029/2006JC003644

Zheng Quanan. 2017. Satellite SAR Detection of Sub-mesoscale Ocean Dynamic Processes. London: World Scientific, 151–169